

A STUDY OF PROCESS INDUCED VOIDS IN RESISTANCE WELDING OF THERMOPLASTIC COMPOSITES

Huajie Shi, Irene Fernandez Villegas and Harald E.N. Bersee

Structural Integrity & Composites, Faculty of Aerospace Engineering,
Delft University of Technology
Kluyverweg 1, 2629HS, Delft, The Netherlands
Emails: H.Shi@tudelft.nl, I.FernandezVillegas@tudelft.nl, and
H.E.N.Bersee@tudelft.nl

Keywords: Polymer-matrix composites, Thermoplastic resin, Joints/joining, Voids

ABSTRACT

Void formation in resistance welding of woven fabric reinforced thermoplastic composites was investigated. Void contents were measured using optical microscopy and digital image process. Uneven void distributions were observed in the joints, and more voids were found in the middle of the joints than the edges. A higher welding pressure was shown to help reduce the void generation. The mechanisms of void formation, in particular fibre de-compaction induced voids and residual moisture induced voids, were analysed. The model estimations were correlated with the experimental results.

1 INTRODUCTION

Voids, or porosities, have been found to be an issue for thermal processing of thermoplastic composites [1-4], in which re-heating of composites is usually a key step. In resistance welding of thermoplastic composite, voids are sometimes observed in the weld line and adherends of the joints [1, 5-7], and they are shown to have a negative effect on the mechanical performance of the joints [1, 8, 9]. Therefore, understanding the mechanisms of void formation in resistance welding is necessary, based on which the welding process could be improved and the presence of voids could be reduced.

Many hypotheses have been proposed in literature for the voids induced during welding of thermoplastic composites. Howie et al. [5] attribute the voids generated in welding of graphite-polyarylsulfone/polysulfone (PAS/PS) composites to the trapped volatiles and overheating of the weld interface. Xiao et al. [3] consider thermal stress as the main cause of the voids induced during induction heating of carbon fibre reinforced polyetheretherketone (CF/PEEK), and a thermal buckling model is developed. Ageorges et al. [1] attribute voids generated in resistance welding of carbon fibre reinforced polyetherimide (CF/PEI) to the de-consolidations of laminates subjected to an inadequate welding pressure, i.e. lower than 0.2 MPa. Ye et al. [10, 11] propose a physical model for void growth in thermal process, and the traction of “de-compaction” of fibre reinforcements is seen as the main resource of void growth in the adherends. Dubé et al. [7] attribute the generation of voids in resistance welding of glass fibre reinforced polyetherimide (GF/PEI) and CF/PEI to two phenomena: (1) polymer squeezing out; (2) low environmental resistance of PEI. However, a comprehensive understanding regarding the mechanisms of voids formation during resistance welding of thermoplastic composites is still needed, in particular respect to the inherent local heating introduced by welding.

In this study, the dominant mechanisms of void formation in resistance welding of GF/PEI are investigated and identified. The void distributions inside the joints are observed using an optical microscope, and the void contents are quantified using digital image processing technique. Analysis of the mechanisms of void formation in adherend is also performed.

2 EXPERIMENTAL DETAILS

2.1 Materials and welding process

The adherends, with a stacking sequence of [(0/90)₄S], were made of eight layers of 8HS woven GF/PEI prepregs, supplied by TenCate, the Netherlands. The GF/PEI laminates were consolidated in a

hot platen press at a processing temperature of 320 °C and a consolidation pressure of 2.0 MPa for 20 minutes. The obtained laminates had a resin volume fraction of around 50%. Adherend plates of 192 mm × 50 mm were cut from the large laminates using a water-cooled diamond saw. A stainless steel mesh, plain woven with a wire diameter of 0.04 mm and gap of 0.09 mm, was used as the heating element. Strips of mesh in 250 mm × 13 mm were cut and used. To provide a resin rich area the mesh strip was sandwiched between two layers of 60 µm thick PEI resin films prior to the welding process.

An in-house developed resistance welding setup (find more information in [9]) was used to weld the joints. The welding energy was provided by a computer controlled power supply unit from Delta Elektronika. The welding process was controlled by a labview program, and the welding parameters, e.g. current, voltage and temperature, were recorded during the welding process. High-density fibre wood blocks were used as the thermal insulators. Predefined appropriate welding parameters [9], a constant power input of 80 kW/m² and a heating time of 55 s, were used to weld all the joints.

2.2 Experimental procedures

Since the generation of voids will lead to an thickness increase in material, the thermal expansion of both GF/PEI composites and PEI polymer was measured using thermomechanical analysis (TMA). PerKinElmer® Diamond TMA was used for the measurement, and the change of thickness with temperature was recorded. The samples were heated up from T_{room} to 290 °C at a heating rate of 2 °C/min; held at 290 °C for 10 min; and cooled down to T_{room} at a cooling rate of 2 °C/min.

The void distributions in joints were inspected using Zeiss Axiovert 40 MAT optical microscope, at a magnification of 2.5×. The cross sections of the centre parts of the joints were consistently used for microscopy in order to rule out the possible “edge effects”. Grayscale images with 256 levels were captured and the void content was calculated using digital image processing, including image trimming, image filtering, thresholding, binaryzation and pixel statistics.

As the PEI polymer tends to absorb moisture from the surroundings until a saturation state is reached, drying test was performed to measure the weight fractions of residual moisture in the GF/PEI laminates. The initial weights of the samples were measured using a micro-gram balance, and then the samples were dried at 135 °C in an oven until reaching a steady weight. The content of residual moisture can be measured by calculating the weight reduction in the drying process.

3 EXPERIMENTAL RESULTS

To define the main causes of void generation, TMA tests were performed on both the openly stored PEI polymer (with residual moisture) and fully dried GF/PEI composites (no residual moisture). As shown in Figure 1, voids were found in both of the specimens after the cycle. These voids should not be caused by resin squeezing flow or thermal buckling, because there was no resin flow or severe temperature gradients in the specimens. Most likely, the residual moisture and fibre de-compaction were the causes of the voids of the PEI and GF/PEI specimens, respectively. In this study, these two causes were studied separately on their contributions to the void formation in resistance welding.

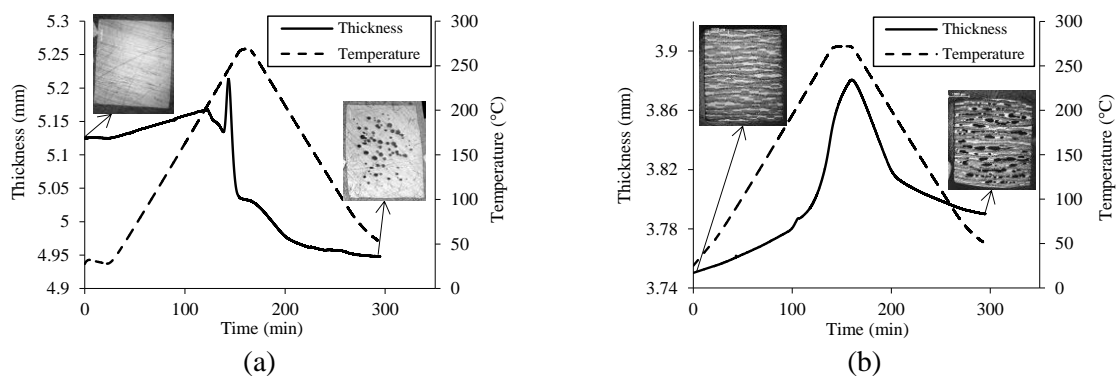


Figure 1: Thermal expansion measurements using thermomechanical analysis for (a) openly stored PEI specimens and (b) fully dried GF/PEI laminates

To investigate the void generation caused by fibre de-compaction, fully dried GF/PEI laminates were used in order to prevent any possible influence of the residual volatiles. The joints were welded under four different welding pressures of 0.1 MPa, 0.2 MPa, 0.4 MPa and 0.8 MPa. As shown in Figures 2 and 3, non-uniform void distributions were observed inside the joints, with more voids concentrated near the middle part of the joints than the edges. The void content was found to decrease with increasing welding pressure, and the joints welded under a welding pressure higher than 0.4 MPa were found to yield a void content of less than 0.1%.

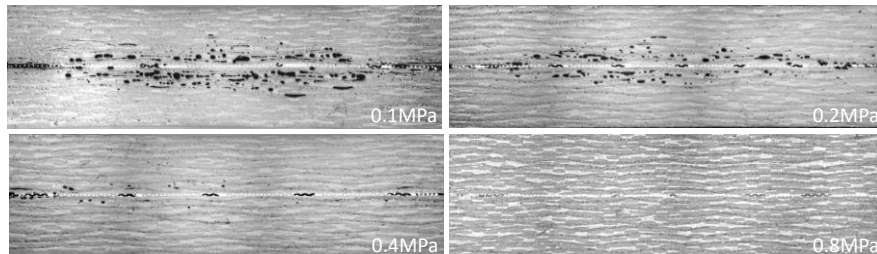


Figure 2: Cross-section micrographs of GF/PEI joints (no residual moisture) welded with different pressure of 0.1 MPa, 0.2 MPa, 0.4 MPa and 0.8 MPa

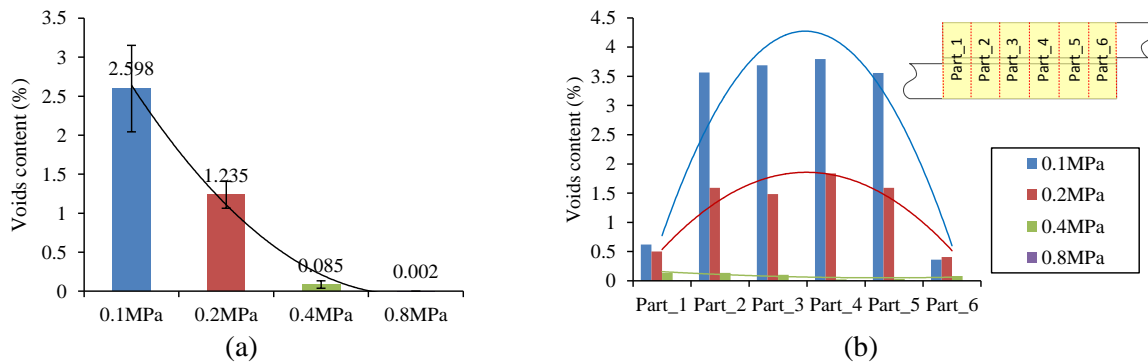


Figure 3: (a) The average void contents and (b) void distributions along the weld overlaps for GF/PEI joints (no residual moisture) welded with different pressures of 0.1 MPa, 0.2 MPa, 0.4 MPa and 0.8 MPa

To investigate the effect of residual moisture on the void generation of resistance welding of GF/PEI joints, the GF/PEI laminates, stored openly in the lab (~ 50% humidity) for more than 1 month, were used. The average weight content of residual moisture in the laminates was measured to be around 0.3 wt%. The joints were welded at different welding pressures of 0.8 MPa, 1.0 MPa, 1.2 MPa and 1.5 MPa. As shown in Figures 4 and 5, the voids were observed to concentrate in the middle parts of the joints rather than the edges, and the void content was found to decrease with welding pressure. A welding pressure of 1.5 MPa was found to effectively reduce the voids content to a relatively low level of around 0.1%.

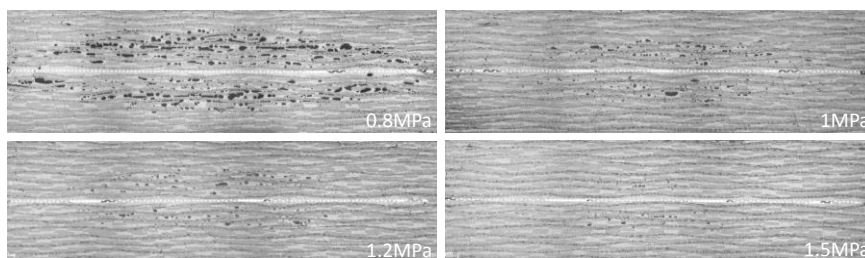


Figure 4. Cross-section micrographs of GF/PEI joints (moisture content \approx 0.3 wt%) welded with different pressures of 0.8 MPa, 1 MPa, 1.2 MPa and 1.5 MPa

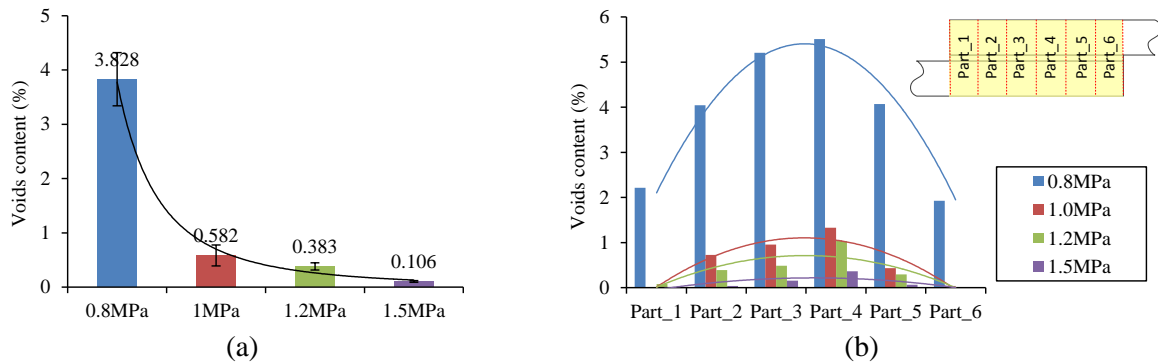


Figure 5: (a) The average void contents and (b) void distributions along the weld overlaps for GF/PEI joints (moisture content ≈ 0.3 wt%) welded with different pressures of 0.8 MPa, 1 MPa, 1.2 MPa and 1.5 MPa

4 ANALYSIS OF VOID FORMATION MECHANISMS

4.1 Fibre de-compaction induced voids

As residual compression stresses can be stored inside the laminates, especially for glass mat or woven fabric reinforced thermoplastic composites [12-15], during consolidation, the stresses may get released when the laminates are re-heated in secondary manufacturing process, such as welding and press forming. Such a process is usually referred to as fibre de-compaction [10], as shown in Figure 6.

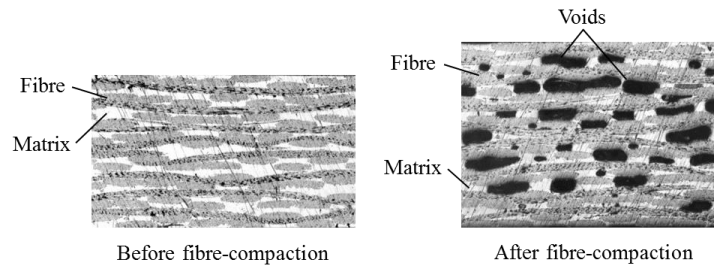


Figure 6: Typical cross-section micrographs of GF/PEI laminate before fibre de-compaction and after fibre de-compaction

Studies have been performed on the fibre de-compaction induced voids in literature [2, 16], and in these studies a representative volume element is usually used with the assumptions: 1) homogeneous material and 2) Darcy's law governed resin flow through the fibre preform. However, for our material system, the voids generated during fibre de-compaction mainly concentrated in the resin rich area but not inside the yarns (see Figure 6), which makes the above assumptions questionable for our material system. Therefore, in the present study, a simple analysis based on the mechanical equilibrium of the compressed fibre was used to describe the process of fibre de-compaction, as shown in Figure 7.

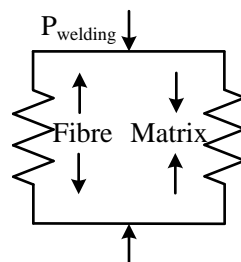


Figure 7: Mechanical equilibrium of the compressed fibre in a composite

At room temperature, the fabric is constrained by the surrounding matrix and the applied welding pressure, which is transferred to the inner stress of the matrix. The mechanical equilibrium can be expressed by the following equation:

$$\sigma_{f0} < UTS_{matrix}(T) + \sigma_{welding} \quad (1)$$

where σ_{f0} is the initial compressive stress of fabric in the consolidated laminate, $UTS_{matrix}(T)$ is the ultimate tensile strength of matrix at temperature T, and $\sigma_{welding}$ is the inner stress of matrix induced by the welding pressure. Since the modulus of matrix decreases with increasing temperature, so does $UTS_{matrix}(T)$. Once $UTS_{matrix}(T)$ drops below σ_{f0} , the fabric could either be de-compacted or be further compressed, and which to happen depends on the value of $\sigma_{welding}$. Fibre de-compaction will happen when equation in below is satisfied

$$\sigma_{f0} > \sigma_{critical} = UTS_{matrix}(T) + \sigma_{welding} \quad (2)$$

As the thickness of laminate H increases with the progress of de-compaction, the fibre volume fraction V_f will decrease:

$$H_0 V_{f0} = H V_f \quad (3)$$

$$(H - H_0)/H = V_v \quad (4)$$

where H_0 is the initial thickness of the laminate, V_{f0} is the initial volume fraction of the fibre, and V_v is the volume fraction of the voids. With the increase of fibre volume fraction, the residual compressive stress of fabric will be continually released until a new equilibrium is reached:

$$\sigma_f = UTS_{matrix}(T) + \sigma_{welding} \approx \sigma_{welding} \quad (5)$$

where σ_f is the residual compressive stress of fabric. With the increase of laminate thickness, voids will fill the incremental volume of the laminate, as shown in Figure 6. As a result, the matrix will become disconnected, especially through the thickness of laminate, and therefore $UTS_{matrix}(T)$ will be released. Therefore $UTS_{matrix}(T)$ can be assumed to be zero, and the final residual stress of fabric, σ_f , should be approximately equal to the external pressure $\sigma_{welding}$. This means that the final de-compaction state should be mainly determined by the applied external pressure and the compressive properties of the fabric, and this conclusion is correlated to the experimental results reported in the literature [16].

The compressibility of glass fabric can be characterized using compression tests, and the compressive stress of the fabric - σ_f can be expressed by a power law function of fibre volume fraction [2, 17, 18]. Eight layers of 7781 glass fabric, 50 mm × 50 mm, were stacked and compressed in a Zwick 20KN machine with a constant cross head speed of 0.05 mm/min. The thickness of the fabric assembly, H, can be converted into fibre volume fraction, V_f , by the equation [12, 14]:

$$V_f = \frac{N_f \rho_a}{\rho_f H} \quad (6)$$

where N_f is the number of the fabric assembly been compressed, ρ_a is the surface density of the fabric and ρ_f is the density of glass fibre. In this study, $N_f = 8$, $\rho_a = 0.3 \text{ kg/m}^2$ [19] and $\rho_f = 2550 \text{ kg/m}^3$ [20]. During the tests, the compression force, or the applied pressure - P, and the thickness of the fabric assembly - H were recorded, and then the relationship between V_f and P can be obtained (by Eq.6), see Figure 8. As the initial fibre volume fraction of the laminates was found to be around 53% ($H_0 = 1.78$ mm), the initial compression pressure of the fabric was calculated to be 0.08 MPa. This means that fibre de-compaction could only happen when the external pressure applied on the fabric was smaller than 0.08 MPa. Assuming the modulus of glass fibre keeps constant during welding, the effect of temperature on the compression pressure of fabric was neglected in the analysis.

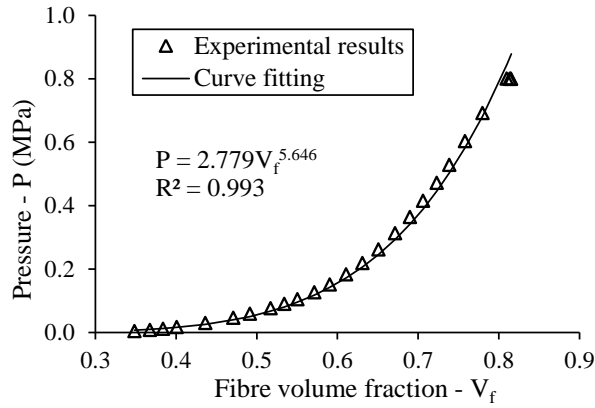
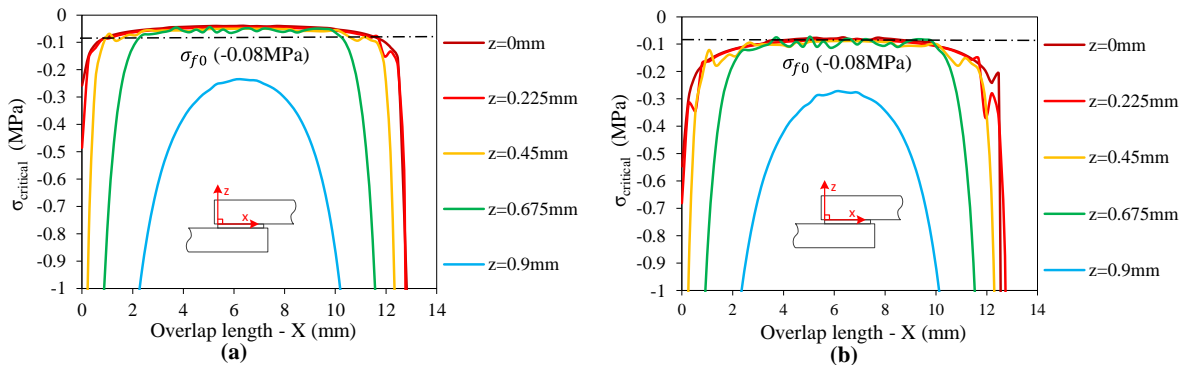


Figure 8: Compressibility of eight layers assembly of 7781 glass fabric

As the stiffness of a thermoplastic matrix is highly dependent on the welding temperature, the welding pressure or internal stress distribution in the joints could also be non-uniform, which in turn will influence void generation and distribution inside the joints. Considering the non-uniform temperature distribution during welding, the distribution of $UTS_{matrix}(T)$ and $\sigma_{welding}$ could also be non-uniform inside the joints as the stiffness of a thermoplastic matrix is highly dependent on the welding temperature. Therefore, the critical stress - $\sigma_{critical}(UTS_{matrix}(T) + \sigma_{welding})$ could vary a lot in the joints. To predict the distributions of temperature and inner stress in the joints during welding, a 2D model of heat transfer and stress analysis was developed (see Appendix A). The distributions of $\sigma_{critical}$ for the joints welded under different welding pressures of 0.1 MPa, 0.2 MPa, 0.4 MPa and 0.8 MPa at the peak welding temperature (at a heating time of 55 s) are shown in Figure 9. The values of critical stresses were found to be higher in the areas near the middle part of the weld overlap than the areas close to the edges, which was believed to be related to the non-uniform temperature distribution in the joints, i.e. welding temperatures are higher in the middle of the joints than the edges [21]. Relatively big oscillations were found in the stress curves, which were probably induced by the big jumps of modulus inside the joints as a result of the existence of big temperature gradients. Having a much lower critical stress in the middle of the weld overlap, fibre de-compaction tends to happen more easily over there. As a consequence, more voids will be generated in the middle part of the joints, which agrees with the experimental results observed in above. Using the initial compressive stress of fabric, 0.08 MPa, as a benchmark, the critical welding pressure needed to prevent the fibre de-compaction induced voids was found to be around 0.4 MPa, which is in correlation with the experimental results.



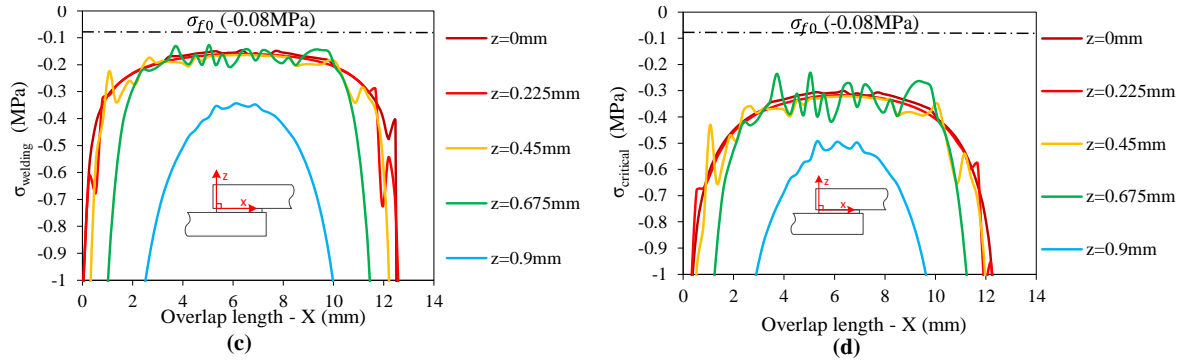


Figure 9: Distributions of critical stress for the GF/PEI joints welded with different pressures of (a) 0.1 MPa, (b) 0.2 MPa, (c) 0.4 MPa and (d) 0.8 MPa (the negative sign in the plots indicates a compressive stress)

4.2 Residual moisture induced voids

The formation of volatile, such as moisture, induced voids can be expressed using classical nucleation theory [22-24]. The distribution of residual volatiles inside the laminates is assumed to be uniform, so homogenous nucleation was used for the analysis. The effect of fibres on void nucleation is un-known, so it is neglected in this study to simplify the problem. The governing equations of homogenous nucleation are [22]:

$$\Delta G = 4\pi R^2 \gamma - \frac{4}{3} \pi R^3 (P_v - P_p) \quad (7)$$

$$R_v^* = 2\gamma / (P_v - P_p) \quad (8)$$

$$\Delta G^* = 16\pi \gamma^3 / 3(P_v - P_p)^2 \quad (9)$$

Where ΔG is Gibbs free energy, R is the radius of the void, γ is the surface tension of polymer-void interface, P_v is the pressure inside the void and P_p is the pressure of the surrounding polymer as a result of the welding pressure, R_v^* is the critical radius of void (the radius corresponding to chemical equilibrium between the void and the surrounding polymer) and ΔG^* is the minimum Gibbs free energy for nucleation of a critical nucleus. The void nucleation rate J can be expressed by [23, 24]:

$$J = N \sqrt{2\gamma/\pi m} \cdot \exp(-16\pi \gamma^3 / 3k_b T (P_v - P_p)^2) \quad (10)$$

where N is the number density of the volatile liquid, m is the mass of a gas molecule, k_b is the Boltzmann constant, 1.38×10^{-23} , and T is the absolute temperature. As void nucleation in the polymer can be assumed to occur instantaneously [25] and the rate of nucleation is proportional to the equilibrium number of critical size voids [24].

After nucleation, voids can grow in polymer, and it can be assumed to be an idea spherical bubble growing in a Newtonian fluid [26, 27]. The governing equation for void growth is given [27]:

$$4\mu \left(\frac{R_0^3 - S_0^3}{S_0^3 + R^3 - R_0^3} \right) \frac{dR}{dt} + \left(\frac{TP_{v0}R_0^3}{T_0R^3} - P_p \right) R - 2\gamma = 0 \quad (11)$$

where R_0 is the initial radius of the void, S_0 is the initial radius of the polymer shell, P_{v0} is the initial pressure inside the void, R is the radius of the void, S is the radius of the polymer shell and μ is the viscosity of the polymer.

Qualitative analysis was performed for the effect of residual moisture on void formation of resistance welding. The effect of welding parameters, i.e. welding temperature and welding pressure, on void nucleation and growth was investigated, and the variables used are listed in Table 1. Arbitrary values were used for R_0 , S_0 and t , because, even though R_0 , S_0 and t influence the void growth rate [25, 28], the trends will remain unchanged. The polymer pressure, P_p , was calculated from the redistributed welding pressure in the composites - $\sigma_{welding}$ by assuming that the welding pressure is transferred mainly to the inner stress of the polymer. The pressure inside the voids, P_v , was assumed to equal to

the vapour pressure of water at a specific temperature. Temperature dependent water vapour pressure [29] was used.

k_b (Boltzman)	γ (N/m)	$N\sqrt{2\gamma/\pi m}$	R_0 (mm)	S_0 (mm)	t (s)
1.38E-23	0.005 ⁽¹⁾	1.13E+25	0.0001	0.1	10

¹ A value taken from the range given in literature [25]

Table 1: Constants used for the analysis of moisture induced void nucleation and growth

As shown in Figure 10, void formation (both void nucleation rate and void growth) can be reduced by using either a lower welding temperature or a higher welding pressure, and the later case has been proved by the experimental results (Figures 4 and 5). Un-even void formation, higher void nucleation rates and faster void growths near the middle of weld overlap than the edges, is predicted in the joints (see Figure 11), which should be related to the higher welding temperature [21] and lower welding pressure in the middle parts of the joints. This prediction shows an agreement with the voids distribution found in the experiments results.

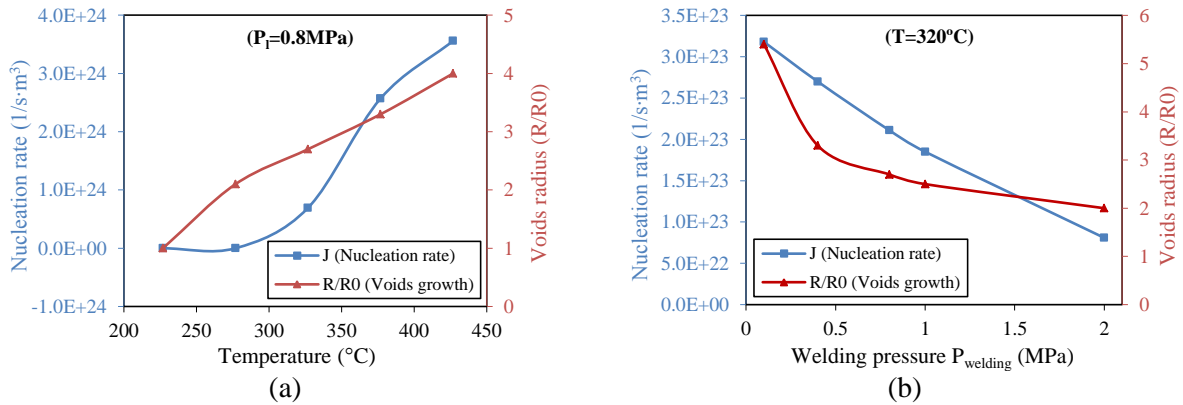


Figure 10: Effects of (a) temperature and (b) welding pressure on void nucleation and growth

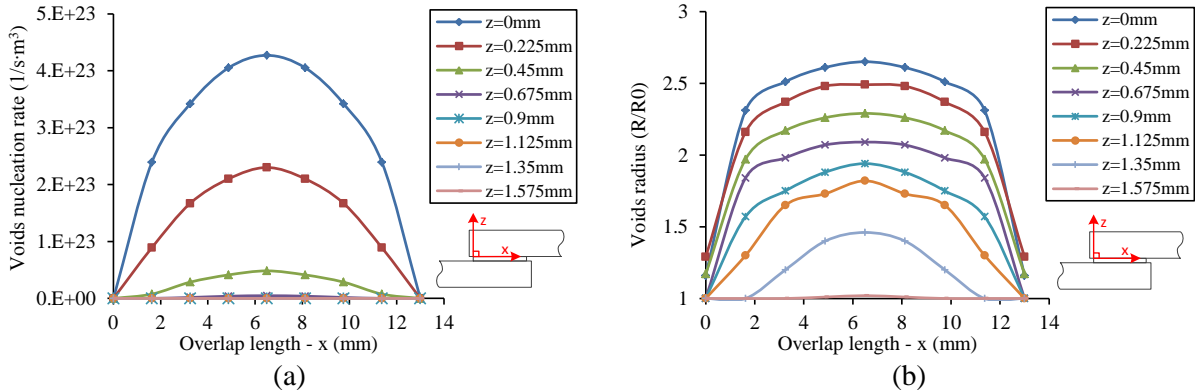


Figure 11: Distributions of (a) void nucleation rate and (b) void growth inside the joints for the maximum welding temperature, $t = 55s$

5 CONCLUSIONS

The void formation in resistance welding of woven glass fabric reinforced polyetherimide (GF/PEI) composites was investigated. A combination of model and experimental analysis was performed to understand the mechanisms of void formation in the welding process.

The void formation in resistance welding was shown to be related to the welding pressure, welding temperature and the material properties of the laminates, i.e. the matrix modulus and the fibre compressibility. Increasing welding pressure was found to help prevent the void generation in general, while a higher welding pressure (1.5 MPa) was required to prevent residual moisture induced voids than the fibre de-compaction induced voids (0.4 MPa). Therefore, the residual moisture induced voids were found to be more critical for welding performed under a moderate welding pressure such as 0.8 MPa.

Due to the non-uniform distribution of temperature in the joints during welding, more voids were found in the middle of the joints than the edges. Future work could be focused on how to improve the uniformity of welding temperature along the weld overlap.

ACKNOWLEDGEMENTS

The first author wishes to acknowledge Jos Sinke for reviewing the paper and providing support for attending the conference. The authors would like to express their gratitude for the support provided by TenCate Advanced Composites, The Netherlands.

APPENDIX A. HEAT TRANSFER ANALYSIS

A 2D heat transfer model was developed using COMSOL Multiphysics® 3.5a. The geometry and boundary conditions were shown in Figure A.12. The free convection coefficient $h = 5 \text{ W/m}^2 \cdot \text{K}$ [30], the ambient temperature $T_{\text{amb}} = 20^\circ\text{C}$ and the surface emissivity $\varepsilon = 0.95$ [30].

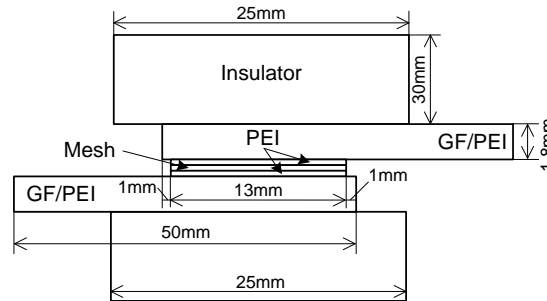


Figure A.12: Geometry and boundary conditions for heat transfer analysis of resistance welding

The relevant material properties are listed in Table A.2. Temperature dependent material properties were used for GF/PEI laminates and PEI film, as listed in Table A.3. The material properties for the PEI were provided by the supplier, and the temperature dependent specific heat of GF/PEI was measured using differential scanning calorimetry (DSC) tests, according to ASTM E1269-11. The temperature dependent thermal conductivity of GF/PEI laminates was measured in the laboratories of the Koninklijke DSM N.V., the Netherlands using the laser flash method.

Material properties	Density	Specific heat	Thermal conductivity		Reference
	ρ (kg/m^3)	C_p ($\text{J/kg}\cdot^\circ\text{C}$)	k_{xx}, k_{yy} ($\text{W/m}\cdot^\circ\text{C}$)	k_{zz} ($\text{W/m}\cdot^\circ\text{C}$)	
Metal mesh	7780	460	10	10	[21]
Wood insulator	1242	1090	0.12	0.12	[21]
PEI resin film	1270	980	0.22	0.22	ρ, k : [31]; C_p : [32]
GF/PEI	1930	890	0.53	0.4	Measured

Table A.2: Material properties at room temperature for heat transfer model

Temperature ($^\circ\text{C}$)	GF/PEI		PEI	
	Specific heat (Measured)	Thermal conductivity (Measured)	Specific heat [21]	Thermal conductivity [21]

	C_p (J/kg·°C)	k_{xx}, k_{yy} (W/m·°C)	k_{zz} (W/m·°C)	C_p (J/kg·°C)	k (W/m·°C)
20	890	0.53	0.4	980	0.22
70	1000	0.57	0.43	1180	0.23
120	1090	0.59	0.44	1360	0.24
170	1150	0.6	0.45	1518	0.25
220	1340	0.65	0.49	1865	0.26
270	1450	0.68	0.38	1963	0.26

Table A.3: Temperature dependent material properties of GF/PEI and PEI

APPENDIX B. STRESS ANALYSIS

Structural analysis, coupled with heat transfer model, was performed to predict the inner stresses in joints during welding. Several assumptions were made: (1) a 2D model in plane strain was used; (2) viscous stress is ignored due to the small strain rate during welding, (3) the weld line was not considered in the model; (4) half model was used due to the symmetry geometry; (5) thermal expansion was not considered in the model. The geometry and boundary conditions of the model are illustrated in Figure B.13. The relevant material properties at room temperature are listed in Table B.4.

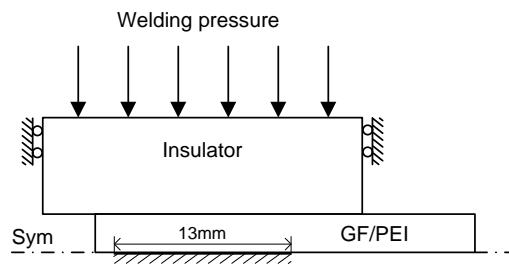


Figure B.13: Geometry and boundary conditions for internal stress analysis

Material	Young's Modulus E (GPa)	Poisson's ratio ν
Wood insulator	12.4 [33]	0.3 [33]
Glass fibre	73 [20]	0.22 [20]
PEI	4.63 (Measured by DMA)	0.36 [31]
GF/PEI	8.71* (Predicted using rules of mixture)	0.3 (Assumption)

* Out-of-plane Modulus

Table B.4: Material properties at room temperature for stress analysis

Temperature dependent modulus was used for GF/PEI. Since the load applied to the laminates was mainly through the thickness of the laminates, compression stress should be the dominate stress of the joints. To simplify the problem, GF/PEI laminate was assumed to be isotropic and the temperature dependent out-of-plane modulus was used. Assuming that the modulus of glass fibre remains constant during the welding process, the temperature dependent out-of-plane modulus of GF/PEI, E_c , was approximately predicted using the rule of mixtures [34]:

$$E_c = \frac{E_f \cdot E_m}{E_m V_f + E_f (1 - V_f)} \quad (\text{B.12})$$

where E_f is the modulus of the fibre and E_m is the modulus of the matrix. Dynamic mechanical analysis (DMA) and rheology measurements were used to measure the modulus of PEI with temperature. The DMA tests were performed from T_{room} to 240 °C with a heating rate of 2.5 °C/min using a frequency swept of 0.1 Hz ~ 100 Hz. As the shear rate of matrix was believed to be low during resistance welding, the results measured with a frequency of 0.1Hz were used. DMA tests cannot measure the

modulus of PEI at a temperature > 240 °C, rheology measurements were performed for high temperatures, and E' (tensile storage modulus) was calculated from G' (shear storage modulus) using an assumed constant Poisson's ratio of 0.3. A temperature sweep was performed by cooling the molten PEI sample from 320 °C at a rate of 1 °C/min until the temperature at which the force limit of the machine was reached, and an angle frequency of 10 rad/s was used. Finally, E_c of the laminates was calculated from the values of E_f and E_m using Eq. (B.12), as listed in Table B.5.

Temperature T (°C)	Storage Modulus of PEI E' (GPa)	Storage Modulus of GF/PEI E' (GPa)
20	4.63	8.71
50	4.26	8.43
100	4.17	7.88
200	3.7	7.03
237	0.07	0.14
270	3.16E-4*	6.32E-4
290	1.78E-4*	3.56E-4
300	1.18E-4*	2.36E-4
310	7.3E-5*	1.46E-4
320	4.3E-5*	8.60E-5

* Calculated using G' by assuming a constant Poisson's ratio of 0.3

TableB.5: The predicted temperature dependent modulus of GF/PEI in the direction through thickness

REFERENCES

- [1] C. Ageorges, L. Ye, M. Hou. Experimental investigation of the resistance welding of thermoplastic-matrix composites. Part II: optimum processing window and mechanical performance. *Composites Science and Technology*. 2000;60(8) pp. 1191-1202.
- [2] J. Wolfrath, V. Michaud, J. Manson. Deconsolidation in glass mat thermoplastic composites: Analysis of the mechanisms. *Composites Part a-Applied Science and Manufacturing*. 2005;36(12) pp. 1608-1616.
- [3] X. Xiao. A model for deconsolidation phenomenon in induction heating of thermoplastic resin composites. *Ninth international conference on composite materials (ICCM9)*. Spain1993. pp. 243-250.
- [4] W. M.D., P. B, E. MJ-A. Void evolution during stamp-forming of thermoplastic composites. *15th International Conference on Composite Materials (ICCM-15)*. Durban, South Africa2005.
- [5] I. Howie, J. Gillespie, A. Smiley. Resistance Welding of Graphite-Polyarylsulfone/Polysulfone Dual-Polymer Composites. *Journal of Thermoplastic Composite Materials*. 1993;6(3):205-25.
- [6] D. Stavrov, H. Bersee. Experimental investigation of resistance welding of thermoplastic composites with metal mesh heating element. *SAMPE-Europe conference proceedings*. Paris, France2004.
- [7] M. Dubé, P. Hubert, J. Gallet, D. Stavrov, H. Bersee, A. Yousefpour. Metal mesh heating element size effect in resistance welding of thermoplastic composites. *Journal of Composite Materials*. 2012;46(8) pp. 911-919.
- [8] F. Henninger, L. Ye, K. Friedrich. Deconsolidation behaviour of glass fibre-polyamide 12 composite sheet material during post-processing. *Plastics Rubber and Composites Processing and Applications*. 1998;27(6) pp. 287-292.
- [9] H. Shi, I. Villegas, H. Bersee. Strength and failure modes in resistance welded thermoplastic composite joints: Effect of fibre-matrix adhesion and fibre orientation. *Composites Part A: Applied Science and Manufacturing*. 2013;55(0) pp. 1-10.
- [10] L. Ye, M. Lu, Y. Mai. Thermal de-consolidation of thermoplastic matrix composites--I. Growth of voids. *Composites Science and Technology*. 2002;62(16):2121-30.

- [11] M. Lu, L. Ye, Y. Mai. Thermal de-consolidation of thermoplastic matrix composites--II. "Migration" of voids and "re-consolidation". *Composites Science and Technology*. 2004;64(2) pp. 191-202.
- [12] Y. Kim, S. McCarthy, J. Fanucci. Compressibility and relaxation of fiber reinforcements during composite processing. *Polymer Composites*. 1991;12(1) pp. 13-19.
- [13] F. Robitaille, R. Gauvin. Compaction of textile reinforcements for composites manufacturing. I: Review of experimental results. *Polymer Composites*. 1998;19(2) pp. 198-216.
- [14] R. Saunders, C. Lekakou, M. Bader. Compression in the processing of polymer composites 1. A mechanical and microstructural study for different glass fabrics and resins. *Composites Science and Technology*. 1999;59(7) pp. 983-993.
- [15] V. Michaud, J. Månson. Impregnation of Compressible Fiber Mats with a Thermoplastic Resin. Part I: Theory. *Journal of Composite Materials*. 2001;35(13) pp. 1150-1173.
- [16] L. Ye, Z. Chen, M. Lu, M. Hou. De-consolidation and re-consolidation in CF/PPS thermoplastic matrix composites. *Composites Part A: Applied Science and Manufacturing*. 2005;36(7) pp. 915-922.
- [17] N. Pearce, J. Summerscales. The compressibility of a reinforcement fabric. *Composites Manufacturing*. 1995;6(1) pp. 15-21.
- [18] R. Saunders, C. Lekakou, M. Bader. Compression in the processing of polymer composites 2. Modelling of the viscoelastic compression of resin-impregnated fibre networks. *Composites Science and Technology*. 1999;59(10) pp. 1483-1494.
- [19] Hexcel. Reinforcements Data Sheets. <http://www.hexcel.com/Resources/Fabrics-Data-Sheets2012>.
- [20] <http://www.matweb.com/search/DataSheet>. E-Glass Fiber, Generic. Matweb. 2012. Oxford, UK: Elsevier; 2007.
- [21] H. Shi, I. Villegas, H. Bersee. Modelling of Heat Transfer and Consolidation For Thermoplastic Composites Resistance Welding. *18th International Conference on Composites Materials. Jeju, South Korea, 2011*.
- [22] J. Colton, N. Suh. The nucleation of microcellular thermoplastic foam with additives: Part I: Theoretical considerations. *Polymer Engineering & Science*. 1987;27(7) pp. 485-92.
- [23] J. Han, C. Dae Han. Bubble nucleation in polymeric liquids. II. theoretical considerations. *Journal of Polymer Science Part B: Polymer Physics*. 1990;28(5) pp. 743-61.
- [24] M. Blander, J. Katz. Bubble nucleation in liquids. *AIChE Journal*. 1975;21(5) pp. 833-848.
- [25] S. Roychowdhury, J. JWG, S. Advani. Volatile-induced Void formation in amorphous thermoplastic polymeric materials : I. Modeling and parametric studies. London, *ROYAUME-UNI: Sage*; 2001.
- [26] A. Arefmanesh, S. Advani, E. Michaelides. An accurate numerical solution for mass diffusion-induced bubble growth in viscous liquids containing limited dissolved gas. *International Journal of Heat and Mass Transfer*. 1992;35(7) pp. 1711-1722.
- [27] S. Ranganathan, S. Advani, M. Lamontia. Non-isothermal process model for consolidation and void reduction during in-situ tow placement of thermoplastic composites. *Journal of Composite Materials*. 1995;29(8) pp. 1040-1062.
- [28] S. Leung, C. Park, D. Xu, H. Li, RG. Fenton. Computer Simulation of Bubble-Growth Phenomena in Foaming. *Industrial & Engineering Chemistry Research*. 2006;45(23): pp. 7823-31.
- [29] Saturated Vapor Pressure. <http://ddbonline.ddbst.com/AntoineCalculation/AntoineCalculationCGI.exe> ed: DDBST GmbH; 2013.
- [30] S. Holmes, J. Gillespie. Thermal Analysis for Resistance Welding of Large-Scale Thermoplastic Composite Joints. *Journal of Reinforced Plastics and Composites*. 1993;12(6) pp. 723-736.
- [31] <http://www.tencate.com>. CETEX® PEI Technical Data. TenCate. 2009.
- [32] Sabic. Thermal conductivity of Ultem 1000 PEI. <http://www.sabic-ip.com/gepapp/eng/eddinter/eddchart>; 2012.
- [33] Predefined Built-In Materials for all COMSOL Modules. www.comsol.nl; 2012.
- [34] V. Vasiliev, E. Morozov. *Advanced Mechanics of Composite Materials (Second Edition)*.